Wei-Wen Yu International Specialty Conference on Cold-Formed Steel Structures
St. Louis, Missouri, U.S.A., November 7 & 8, 2018

Distortional Buckling of Cold-Formed Steel Flanges Under Stress Gradient

Robert S. Glauz, P.E.[1]

Abstract

The strength of cold-formed steel beams with stiffened flanges may be controlled by distortional buckling. Buckling stress prediction methods have been developed for flanges under uniform compression. However, channel sections are commonly used where bending occurs about the minor axis with flanges under stress gradient, such that the edges are in compression and the flanges may experience distortional buckling. Current design specifications do not explicitly address this failure mode, which could lead to unsafe designs. This paper presents and verifies an analytical approach for distortional buckling stress prediction for flanges under stress gradient. The approach is consistent with the design method used for flanges under uniform compression to facilitate straightforward incorporation into design specifications.

Introduction

Distortional buckling is a potential failure mode for cold-formed steel members of open cross-sections, where an entire stiffened compression flange becomes unstable. Analytical methods for predicting this complex behavior have been developed for compression members by Lau and Hancock (1987) and extended to flexural members by Hancock (1995, 1997). Subsequent work by Schafer and Peköz (1999), Schafer (2002), and Schafer et al. (2006) provided more rigorous treatments for distortional buckling strength prediction.

The American Iron and Steel Institute (AISI) Specification for the design of cold-formed steel structural members (AISI 2016) supports two methods of predicting the elastic distortional buckling stresses of stiffened flanges. Numerical methods such as finite strip analysis provide elastic buckling solutions for any general case, but require specialized software not yet widely used in cold-formed steel design.

[1] President/Owner, RSG Software, Inc., Lee's Summit, Missouri, USA

AISI also provides analytical solutions which permit the direct (although complex) calculation of distortional buckling stress predictions, based on the work by Schafer et al. (1999, 2002, 2006). Currently, these hand methods are given for compression members, and for flexural members having a flange under uniform compression. They are commonly used for channel section studs, girts, and joists.

Channels, hat sections, and many custom shapes can experience bending about the axis perpendicular to the flange, which may also be subject to distortional buckling. Figure 1(a) illustrates distortional buckling for major axis bending, where the flange has uniform compression. Figures 1(b) and 1(c) show examples of minor axis bending with the flanges under stress gradient.

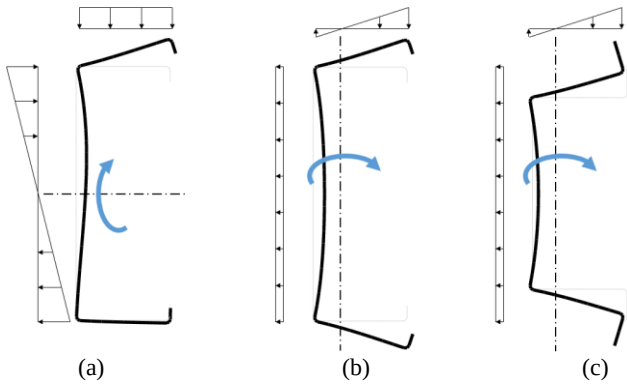

Figure 1. Distortional buckling of flanges under major and minor axis bending

Teng et al. (2003) studied distortional buckling behavior for channel section beam-columns with particular attention to bending in the plane of symmetry. This theoretical work provided a complex analytical approach and requires iteration on the half-wavelength to establish the critical buckling moment.

The lack of a direct hand solution for these minor axis bending cases may result in oversight by the engineer of this potential distortional buckling failure mode. This paper presents an analytical method for the prediction of elastic distortional buckling stresses for flanges under stress gradient, with verification against numerical solutions permitted by the AISI Specification.

Distortional Buckling Prediction

Distortional buckling involves primarily rotation of the flange and distortion of the web. Prediction of the elastic distortional buckling stress requires analysis of

the flexural-torsional buckling behavior of the flange, combined with the rotational resistance provided by the web. The method used in Schafer and Peköz (1999) was to analyze the flange as a column and the web as a finite strip element. The same approach is extended here for the case of a flange under a stress gradient.

The rotational stiffness demanded by the flange involves an elastic rotational stiffness component ($k_{\phi fe}$) and a stress-dependent geometric rotational stiffness component ($\tilde{k}_{\phi fg}$), which takes the form shown in Eq. 1. This is the negative of the stiffness *provided by* the flange. The rotational stiffness provided by the web also involves an elastic rotational stiffness component ($k_{\phi we}$) and a stress-dependent geometric rotational stiffness component ($\tilde{k}_{\phi fg}$), as shown in Eq. 2.

$$k_{\phi f} = \tilde{k}_{\phi fg} f_{crd} - k_{\phi fe} \quad (1)$$

$$k_{\phi w} = k_{\phi we} - \tilde{k}_{\phi wg} f_{crd} \quad (2)$$

Equating the rotational stiffness demanded by the flange to the rotational stiffness provided by the web gives the critical distortional buckling stress of the flange/web system.

$$f_{crd} = \frac{k_{\phi fe} + k_{\phi we}}{\tilde{k}_{\phi fg} + \tilde{k}_{\phi wg}} \quad (3)$$

Flange Rotational Stiffness

The flange is analyzed as a beam-column as illustrated in Figure 2. The flange/web juncture at **h** is resisted rotationally by a spring of stiffness $k_{\phi f}$, and is

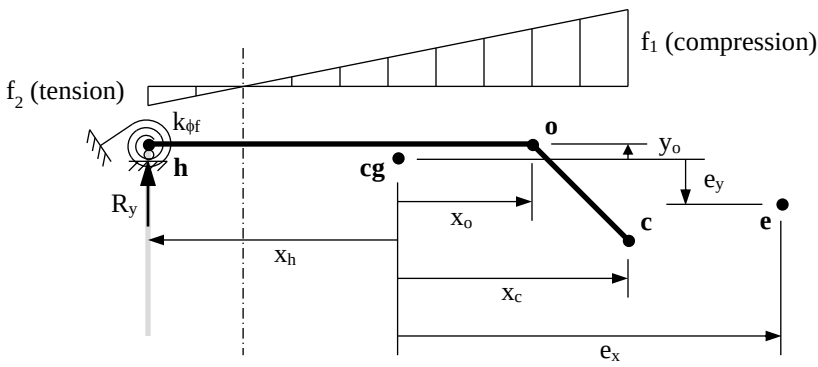

Figure 2. Flange under stress gradient

supported in the direction of the web with force R_y. An axial force P is applied at point **e**, producing the stress distribution equivalent to bending about the centroidal y axis of the entire section.

The centroid of the flange is identified as **cg**, the shear center of the flange is at **o**, and the extreme compression fiber of the flange is at **c**. The differential equations of equilibrium are:

$$EI_{yf}u'''' + EI_{xyf}v'''' + Pu'' + P(y_o - e_y)\phi'' = 0 \quad (4)$$

$$EI_{xf}v'''' + EI_{xyf}u'''' + Pv'' - P(x_o - e_x)\phi'' - R_y = 0 \quad (5)$$

$$EC_{wf}\phi'''' - \left(GJ_f - 2\beta_{yf}Pe_y - 2\beta_{xf}Pe_x - \frac{I_{of}}{A_f}P\right)\phi'' + P(y_o - e_y)u'' - P(x_o - e_x)v'' + R_y(x_o - x_h) + k_{\phi f}\phi = 0 \quad (6)$$

where A_f, I_{xf}, I_{yf}, I_{xyf}, I_{of}, C_{wf}, J_f, β_{xf}, and β_{yf} are section properties of the flange. The following shape functions are assigned, consistent with a simply supported column:

$$\phi = A_1 \sin\frac{\pi z}{L}, \quad u = A_2 \sin\frac{\pi z}{L}, \quad v = (x_o - x_h)A_1 \sin\frac{\pi z}{L} \quad (7a,b,c)$$

The stresses f_1 and f_2 can be expressed in terms of P, e_x, and flange section properties as shown in Eq. 8. It is also convenient to define expressions for flange stress gradient ξ_f and flange stress ratio ψ_f.

$$f_1 = \frac{P}{A_f} + \frac{Pe_x x_c}{I_{yf}}, \quad f_2 = \frac{P}{A_f} + \frac{Pe_x x_h}{I_{yf}} \quad (8a,b)$$

$$\xi_f = (f_1 - f_2)/f_1 \quad (9)$$

$$\psi_f = \frac{f_{cg}}{f_1} = 1 - \xi_f \frac{x_c}{x_c - x_h} \quad (10)$$

From these relationships, the applied axial force and moments can be stated as:

$$P = A_f\psi_f f_1, \quad Pe_x = \frac{I_{yf}}{x_c - x_h}\xi_f f_1, \quad Pe_y = \frac{I_{xyf}}{x_c - x_h}\xi_f f_1 \quad (11a,b,c)$$

Substituting the shape functions from Eq. 7 into Eq. 4 provides a relationship between the magnitudes of translation (u) and rotation (ϕ) shown in Eq. 12. The denominator consists of an Euler buckling term and the flange load P. This flange load is generally much less than the flange buckling load about the y axis, and can be neglected to simplify the solution.

$$\frac{A_2}{A_1} = \frac{\frac{\pi^2}{L^2}EI_{xyf}(x_o - x_h) - A_f y_o \psi_f f_1 + \frac{I_{xyf}}{x_c - x_h}\xi_f f_1}{\frac{\pi^2}{L^2}EI_{yf} - A_f \psi_f f_1} \tag{12}$$

Eq. 5 provides an expression for R_y which can be substituted into Eq. 6. Then substituting the shape functions from Eq. 7 into the result, utilizing Eq. 12 with the simplified denominator, and neglecting the f_1^2 terms produces an expression for $k_{\phi f}$ in the form of Eq. 1. The resulting rotational stiffness components are:

$$k_{\phi fe} = \frac{\pi^4}{L^4}\left[EC_{wf} + EI_{xf}(x_o - x_h)^2\left(1 - \frac{I_{xyf}^2}{I_{xf}I_{yf}}\right)\right] + \frac{\pi^2}{L^2}GJ_f \tag{13}$$

$$\tilde{k}_{\phi fg} = \frac{\pi^2}{L^2}\left[I_{xf} + I_{yf} + A_f(y_o^2 + x_h^2) - 2A_f y_o(x_o - x_h)\frac{I_{xyf}}{I_{yf}}\right]\psi_f + \frac{\pi^2}{L^2}\left[2I_{yf}\left(\frac{\beta_{xf} + x_o - x_h}{x_c - x_h}\right) + 2I_{xyf}\left(\frac{\beta_{yf} + (x_o - x_h)I_{xyf}/I_{yf}}{x_c - x_h}\right)\right]\xi_f \tag{14}$$

Eq. 13 is identical to that used in the AISI Specification. A special case of Eq. 14 with uniform compression on the flange, where $\psi_f = 1$ and $\xi_f = 0$, is shown as Eq. 15. This is the same as the equation in the AISI Specification, except one negligible term is omitted here due to the simplification made using Eq. 12.

$$\tilde{k}_{\phi fg} = \frac{\pi^2}{L^2}\left[I_{xf} + I_{yf} + A_f(y_o^2 + x_h^2) - 2A_f y_o(x_o - x_h)\frac{I_{xyf}}{I_{yf}}\right] \tag{15}$$

The properties β_{xf} and β_{yf} can be difficult to calculate for complex flanges, so it is beneficial to make some simplifying approximations if the error is small. For a typical flange as shown in Figure 2, $\beta_{xf} + x_o - x_h$ is generally slightly less than $0.5(x_c - x_h)$, and the I_{xyf} term is small relative to the I_{yf} term. From these observations, Eq. 14 can be simplified to the following with reasonable accuracy:

$$\tilde{k}_{\phi fg} = \frac{\pi^2}{L^2}\left[I_{xf} + I_{yf} + A_f(y_o^2 + x_h^2) - 2A_f y_o(x_o - x_h)\frac{I_{xyf}}{I_{yf}}\right]\psi_f + \frac{\pi^2}{L^2}I_{yf}\xi_f \tag{16}$$

Web Rotational Stiffness

Utilizing the same approach as Schafer and Peköz (1999), the rotational resistance provided by the web is derived using a single finite strip as shown in Figure 3. For the common case of a symmetrical channel or hat section, the web is under uniform tension where $f_3 = f_2$ and $\theta_2 = -\theta_1$.

Following the same development, M_1 and M_2 are the nodal moments calculated by Eq. 17 and Eq. 18, using the stiffness coefficients for a finite strip as defined in Cheung (1976). The following stiffness coefficient equivalencies are also recognized: $k_{24e} = k_{42e}$, $k_{24g} = k_{42g}$, $k_{22e} = k_{44e}$.

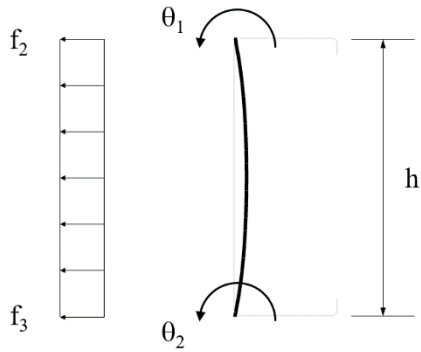

Figure 3. Web finite strip

$$M_1 = (k_{22e} - k_{22g})\theta_1 + (k_{24e} - k_{24g})\theta_2 \quad (17)$$

$$M_2 = (k_{42e} - k_{42g})\theta_1 + (k_{44e} - k_{44g})\theta_2 \quad (18)$$

For the symmetrical case, the rotational stiffness provided by the web is straight-forward, and separation into the elastic stiffness and geometric stiffness components is evident.

$$M_1 = (k_{22e} - k_{22g})\theta_1 - (k_{24e} - k_{24g})\theta_1 = \frac{L}{2}k_{\phi w}\theta_1 \quad (19)$$

$$k_{\phi we} = \frac{2}{L}(k_{22e} - k_{24e}) \quad (20)$$

$$k_{\phi wg} = \frac{2}{L}(k_{22g} - k_{24g}) \quad (21)$$

Incorporating the expressions for the stiffness coefficients using Poisson's ratio for steel of 0.3 provides the following relationships:

$$\frac{2}{L}k_{22e} = \frac{Et^3}{12h(1-\mu^2)}\left[4 + \frac{4}{15}\left(\frac{\pi h}{L}\right)^2 + \frac{1}{105}\left(\frac{\pi h}{L}\right)^4\right] \quad (22)$$

$$\frac{2}{L}k_{24e} = \frac{Et^3}{12h(1-\mu^2)}\left[2 - \frac{1}{15}\left(\frac{\pi h}{L}\right)^2 - \frac{1}{140}\left(\frac{\pi h}{L}\right)^4\right] \quad (23)$$

$$\frac{2}{L}k_{22g} = \frac{\pi^2 th^3}{1680L^2}[10 + 6(1 - \xi_w)]f_2 \quad (24)$$

$$\frac{2}{L}k_{24g} = -\frac{\pi^2 th^3}{1680L^2}[6 + 6(1 - \xi_w)]f_2 \quad (25)$$

The web stress gradient ξ_w is defined as $(f_2 - f_3) / f_2$, and is zero for the symmetrical case. The stress f_2 can be expressed as $(1 - \xi_f)f_1$. The resulting stiffness components are then given as:

$$k_{\phi we} = \frac{Et^3}{6h(1-\mu^2)}\left[1 + \frac{1}{6}\left(\frac{\pi h}{L}\right)^2 + \frac{1}{120}\left(\frac{\pi h}{L}\right)^4\right] \tag{26}$$

$$\tilde{k}_{\phi wg} = \frac{\pi^2}{L^2}\frac{th^3}{60}(1 - \xi_f) \tag{27}$$

Critical Buckling Length

The rotational stiffness components derived for the flange and web are functions of the half-wavelength L, as shown in condensed form below. Substituting these into the critical buckling stress Eq. 3 results in Eq. 30.

$$k_{\phi fe} = C_1 L^{-4} + C_2 L^{-2}, \quad \tilde{k}_{\phi fg} = C_3 L^{-2} \tag{28a,b}$$

$$k_{\phi we} = K_1 + K_2 L^{-2} + K_3 L^{-4}, \quad \tilde{k}_{\phi wg} = K_4 L^{-2} \tag{29a,b}$$

$$f_{crd} = \frac{C_1 L^{-2} + C_2 + K_1 L^2 + K_2 + K_3 L^{-2}}{C_3 + K_4} \tag{30}$$

Setting the derivative equal to zero provides the buckling length at which the buckling stress is minimized. Substituting the appropriate terms for C_1, K_3, and K_1 gives the critical buckling length as Eq. 32.

$$\frac{df_{crd}}{dL} = \frac{-2C_1 L^{-3} + 2K_1 L - 2K_3 L^{-3}}{C_3 + K_4} = 0 \longrightarrow L_{crd} = \left(\frac{C_1 + K_3}{K_1}\right)^{1/4} \tag{31}$$

$$L_{crd} = \pi h \left\{\frac{6(1-\mu^2)}{t^3 h^3}\left[C_{wf} + I_{xf}(x_o - x_h)^2\left(1 - \frac{I_{xyf}^2}{I_{xf} I_{yf}}\right)\right] + \frac{1}{120}\right\}^{1/4} \tag{32}$$

Web in Tension

Numerical analyses of various sections with flanges under stress gradient revealed that the web depth, h, has little influence on either the critical buckling length or the elastic buckling stress. The above derived equations did not reflect that trend and overestimated the buckling stress.

Figure 4(a) shows the relationship between rotational stiffness and longitudinal strain based on a single finite strip, for h/t = 80 and various values of h/L. The

rotational stiffness is quantified as the dimensionless $k_{\phi w}h/D$, where D is the plate rigidity $Et^3/12(1-\mu^2)$. Teng et al. (2003) developed a more comprehensive solution for the web rotational stiffness based on the plate theory work by Timoshenko (1959). Figure 4(b) plots this solution and illustrates how the rotational stiffness is much different from the single finite strip simplification in the tension region.

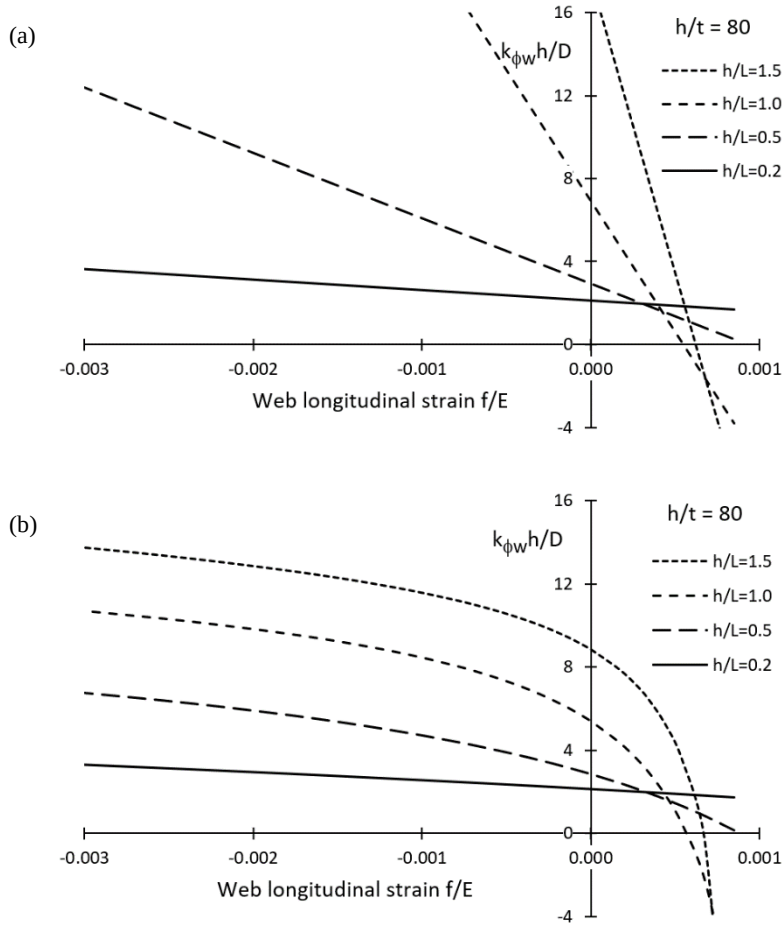

Figure 4. Web rotational stiffness: (a) Finite strip model (b) Teng et al. solution

The direct solution approach utilizing Eq. 3 requires a linear relationship between stress and stiffness in the tension region. At first glance, a linear approximation seems feasible, although the stiffness equation is quite complex.

$$k_{\phi w} = \frac{D}{h}\frac{2\alpha\beta\left[1+\tanh^2(\alpha/2)\tan^2(\beta/2)\right]}{\alpha[1-\tanh^2(\alpha/2)]\tan(\beta/2)+\beta[1+\tan^2(\beta/2)]\tanh(\alpha/2)} \tag{33}$$

where

$$\alpha = \frac{\pi}{\sqrt{2}}\frac{h}{L}\left[1+\sqrt{1+K(L/h)^2}\right]^{1/2} \tag{34}$$

$$\beta = \frac{\pi}{\sqrt{2}}\sqrt{K}\left[1+\sqrt{1+K(L/h)^2}\right]^{-1/2} \tag{35}$$

$$K = -\frac{th^2 f}{\pi^2 D} \tag{36}$$

Some simplification can be achieved by observing the stiffness relationship where β is a multiple of π ($\beta=n\pi$). For even values of n, $\tan(\beta/2)$ vanishes. For odd values of n, $1/\tan(\beta/2)$ vanishes. Then the following relationships exist:

$$\alpha = \frac{\pi h}{2nL}\sqrt{K} = n\pi\sqrt{1+(h/nL)^2} \tag{37}$$

$$f = \frac{-4\pi^2 n^4 L^2 D}{th^4}[1+(h/nL)^2] \tag{38}$$

$$k_{\phi w} = \frac{D}{h}2\alpha\tanh^{\pm 1}(\alpha/2) \cong \frac{D}{h}2\alpha = \frac{D}{h}2n\pi\sqrt{1+(h/nL)^2} \tag{39}$$

$$\tilde{k}_{\phi wg} = -\frac{dk_{\phi w}}{df} \cong \frac{k_{\phi w}}{4f} \tag{40}$$

For $\alpha/2 > \pi$, the hyperbolic tangent is nearly 1 and the approximation used in Eq. 39 is applicable. As n increases, the stiffness becomes proportional to Dn/h, and utilizing Eq. 38, it becomes proportional to $t^{5/2}L^{-1/2}E^{3/4}f^{1/4}$. The stiffness is *independent* of h, which agrees with findings from numerical analyses. The geometric stiffness can be determined as the derivative with respect to stress, and the same approximations have been applied in Eq. 40. The geometric stiffness therefore becomes proportional to $t^{5/2}L^{-1/2}E^{3/4}f^{-3/4}$, and is also independent of h. To establish a linear relationship, a representative stress must be chosen, and error increases as the stress deviates from the chosen value.

At lower stresses ($\beta<\pi$) and for determining the elastic stiffness (at $\beta=0$), the above approximations cannot be used. It is observed in Figure 4(b) that for larger h/L values, the stiffness increases roughly proportional to h/L, and the slopes are roughly parallel. This complicates the direct calculation of the critical buckling length. In place of Eq. 29, the forms $k_{\phi we}=K_1+K_2L^{-1}$ and $\tilde{k}_{\phi wg}=K_4L^{-1/2}$ or $\tilde{k}_{\phi wg}=K_4$ produce a higher order polynomial for L_{crd} which prevents a direct solution. Due to these complications, an entirely different approach was pursued.

Since the web depth has little influence on the critical buckling length, an effective web depth can be back-calculated for a given flange configuration using Eq. 32 with the critical buckling length from numerical analysis. This effective web depth can then be used in Eq. 26 to determine $k_{\phi we}$ (at zero stress). For a web in tension, the geometric stiffness is relatively small and can conservatively be approximated as zero. This is particularly true for small h/L which was generally the case for the effective web depth.

A method of estimating the effective web depth is required. Parametric analysis showed that the effective web depth correlates predominantly with the size of the flange. Various measures of flange size were evaluated and the best prediction utilized the radius of gyration of the flange about the axis of the web. An effective web depth of 3.5 times this radius of gyration provided good results.

$$h = 3.5\sqrt{\frac{I_{yf}}{A_f} + x_h^2} \tag{41}$$

Web under Stress Gradient

Some shapes can experience stress gradients in both the flange and web, such as those in Figure 5. It is therefore important to understand how the web stress gradient affects these distortional buckling predictions.

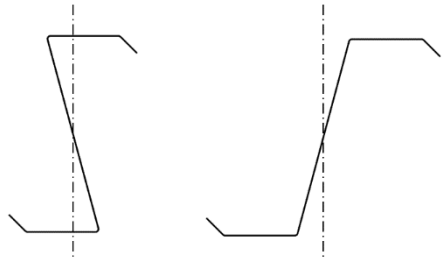

Figure 5. Shapes having web under stress gradient

The derivations above for the web rotational stiffness components relied on symmetry and uniform stress. For a web under stress gradient, an approximation could be made by carrying the ξ_w terms from Eq. 24 and 25 into Eq. 27. This results in a multiplier of $(1 - \frac{3}{7}\xi_w)$, which is only accurate for symmetrical buckling where $\theta_2 = -\theta_1$. The equations shown in Table 1 demonstrate that as the magnitude of θ_2 decreases, the elastic stiffness increases, and the geometric stiffness may decrease or increase depending on the signs of $(2 - \xi_w)$ and $(1 - \xi_f)$.

Table 1: Relationship between node rotation and web stiffness

θ_2/θ_1	$k_{\phi we}$	$\tilde{k}_{\phi wg}$
–1.0	$\frac{Et^3}{12h(1-\mu^2)}\left[2+\frac{10}{30}\left(\frac{\pi h}{L}\right)^2+\frac{14}{840}\left(\frac{\pi h}{L}\right)^4\right]$	$\frac{\pi^2}{L^2}\frac{th^3}{1680}[4+12(2-\xi_w)](1-\xi_f)$
–0.5	$\frac{Et^3}{12h(1-\mu^2)}\left[3+\frac{9}{30}\left(\frac{\pi h}{L}\right)^2+\frac{11}{840}\left(\frac{\pi h}{L}\right)^4\right]$	$\frac{\pi^2}{L^2}\frac{th^3}{1680}[4+9(2-\xi_w)](1-\xi_f)$
0	$\frac{Et^3}{12h(1-\mu^2)}\left[4+\frac{8}{30}\left(\frac{\pi h}{L}\right)^2+\frac{8}{840}\left(\frac{\pi h}{L}\right)^4\right]$	$\frac{\pi^2}{L^2}\frac{th^3}{1680}[4+6(2-\xi_w)](1-\xi_f)$

Incorporating the relative node rotation into concise equations for the rotational stiffness components is challenging. Consider the web behavior where only one flange buckles. The moment M_2 in Eq. 18 is zero and the rotation relationship is:

$$\theta_2 = \frac{-(k_{42e}-k_{42g})}{(k_{44e}-k_{44g})}\theta_1 \tag{42}$$

The solution requires some simplification and approximation to be useful. Schafer and Peköz (1999) used a rational approach, but alternate approaches may offer some improvements. Substituting Eq. 42 into Eq. 19 gives Eq. 43, where the elastic component at zero stress is Eq. 44.

$$k_{\phi w} = \frac{2}{L}\left[\left(k_{22e}-k_{22g}\right)-\frac{(k_{24e}-k_{24g})^2}{k_{22e}-k_{44g}}\right] \tag{43}$$

$$k_{\phi we} = \frac{2}{L}\left(k_{22e}-\frac{k_{24e}^2}{k_{22e}}\right) \tag{44}$$

Simplification is realized using polynomial division with Eq. 23 squared and Eq. 22 to produce Eq. 45. The last term was adjusted to compensate for dropped higher order terms. The resulting Eq. 46 closely matches Eq. 44 for h/L values less than 2.

$$\frac{2}{L}\frac{k_{24e}^2}{k_{22e}} = \frac{Et^3}{12h(1-\mu^2)}\left[1-\frac{2}{15}\left(\frac{\pi h}{L}\right)^2+\frac{3}{560}\left(\frac{\pi h}{L}\right)^4\right] \tag{45}$$

$$k_{\phi we} = \frac{Et^3}{4h(1-\mu^2)}\left[1+\frac{2}{15}\left(\frac{\pi h}{L}\right)^2+\frac{1}{720}\left(\frac{\pi h}{L}\right)^4\right] \tag{46}$$

For the geometric stiffness, it can be assumed that $k_{44g} << k_{22e}$ at the stresses of interest, and can be neglected. Then disregarding the k_{24g}^2 stress term reduces the geometric stiffness to Eq. 47, which permits direct derivation of Eq. 48.

$$k_{\phi wg} = \frac{2}{L}\left(\frac{k_{22e}k_{22g} - 2k_{24e}k_{24g}}{k_{22e}}\right) \tag{47}$$

$$\tilde{k}_{\phi wg} = \frac{\pi^2}{L^2}\frac{th^3}{1680}\left[4 + \frac{5040 + 84\left(\frac{\pi h}{L}\right)^2 - 3\left(\frac{\pi h}{L}\right)^4}{420 + 28\left(\frac{\pi h}{L}\right)^2 + \left(\frac{\pi h}{L}\right)^4}(2 - \xi_w)\right](1 - \xi_f) \tag{48}$$

For many cases, Eq. 48 is more accurate than the current AISI equation. But for large values of h/L (greater than 2), Eq. 48 produces more error. The minimum value of L_{crd} is $\pi h/\sqrt[4]{720}$, or h/L < 1.65, so the above equation is quite suitable. But an alternative is to simplify the AISI equation by dropping a negligible ξ_w term and using the form:

$$\tilde{k}_{\phi wg} = \frac{\pi^2}{L^2}\frac{th^3}{240}\left[\frac{1920 - 810\xi_w + 8\left(\frac{\pi h}{L}\right)^2 + \left(\frac{\pi h}{L}\right)^4}{420 + 28\left(\frac{\pi h}{L}\right)^2 + \left(\frac{\pi h}{L}\right)^4}\right](1 - \xi_f) \tag{49}$$

It should also be noted that sections with sloped webs as in Figure 5 require the flange stiffness components to be determined using a local x axis for the flange which is perpendicular to the web. This ensures that the equations of equilibrium (4-6) for the flange are still satisfied.

Verification

Distortional buckling predictions using the analytical equations developed above were compared to numerical analysis results for a variety of sections. The AISI Specification permits the use of numerical methods, so it is important for the analytical method to produce similar results. The verifications performed in this study used the finite strip method (FSM) in the CFS® software for comparison.

The first set of verifications used symmetrical channel sections having flanges with simple lip stiffeners. Table 2 enumerates the geometry for 60 sections with a material thickness of 1 mm (0.0394 in). This is the same set of sections used in the Schafer and Peköz (1999) study.

Table 3 summarizes the results of the verifications using three sets of equations for the stiffness components. Equation set 1 uses the derived equations in unaltered form, which revealed the flaws in using a single finite element for a web in tension. Equation set 2 applies the effective web depth concept and uses $\tilde{k}_{\phi wg} = 0$. Equation set 3 uses the simplified form for $\tilde{k}_{\phi fg}$ in Eq. 16, which resulted

in a more accurate average F_{pred} and an improved standard deviation. This equation set was then used for verifying other sections.

Table 2: Simple lip section dimensions

Web (mm)	Flange (mm)	Lip (mm)	θ (deg)
50	25	6.25, 12.5	45, 90
100	25	6.25, 12.5	45, 90
	50	6.25, 12.5, 25	45, 90
150	25	6.25, 12.5	45, 90
	50	6.25, 12.5, 25	45, 90
	75	6.25, 12.5, 25, 37.5	45, 90
200	25	6.25, 12.5	45, 90
	50	6.25, 12.5, 25	45, 90
	75	6.25, 12.5, 25, 37.5	45, 90
	100	6.25, 12.5, 25, 37.5, 50	45, 90

Table 3: Performance of distortional buckling prediction equations

	Simple Lip Stiffener			Intermediate Stiffener	Complex Stiffener	Web Hole
Equation Set:	1	2	3	3	3	3
$k_{\phi fe}$	Eq. 13	Eq. 13	Eq. 13	Eq. 13	Eq. 13	Eq. 13
$\tilde{k}_{\phi fg}$	Eq. 14	Eq. 14	Eq. 16	Eq. 16	Eq. 16	Eq. 16
$k_{\phi we}$	Eq. 26	Eq. 26[a]	Eq. 26[a]	Eq. 26[a]	Eq. 26[a]	Eq. 26[a]
$\tilde{k}_{\phi wg}$	Eq. 27	0	0	0	0	0
F_{pred}/F_{FSM}	1.437	0.918	0.940	0.987	0.961	0.922
Std Dev	0.719	0.069	0.048	0.036	0.067	0.050

[a] using Eq. 41 for h

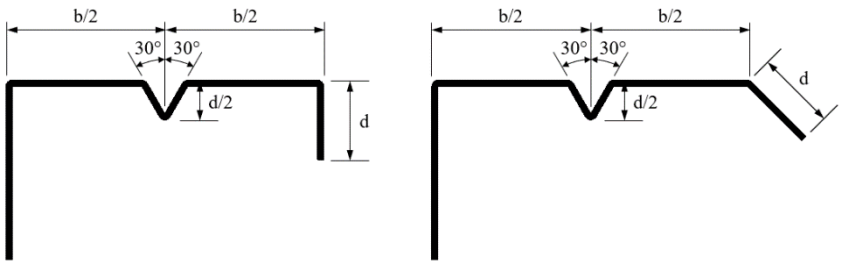

Figure 6. Intermediate stiffener geometry

The sections in Table 2 were analyzed with intermediate flange stiffeners. Figure 6 illustrates the geometry of the stiffener at the middle of the flange, where the

depth of the stiffener is half the lip length. The same equation set 3 produced good results with an average ratio to FSM near 1.0 and a low standard deviation.

A variety of complex flange stiffeners are often used to enhance the stability of the lip, such as those shown in Figure 7. These shapes are also susceptible to distortional buckling when bending about the minor axis. Equation set 3 was utilized again for these shapes, where two flange lengths and two web depths were considered for each. The predictions for these 32 sections also produced good results with a slightly conservative average ratio and a satisfactory standard deviation, as shown in Table 3.

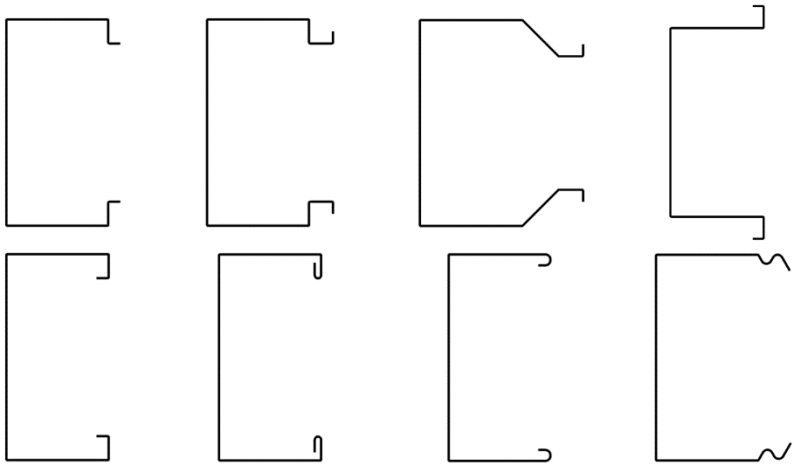

Figure 7. Complex stiffener examples

The AISI Specification has provisions for reducing the distortional buckling stress for webs with holes. The method is to reduce the effective thickness of the web based on the hole length and the distortional buckling half-wavelength. This approximation is applied to both numerical and analytical methods for flanges under uniform compression. It is important to check this method as applied to flanges under stress gradient.

Each of the sections in Table 2 was analyzed with a web hole having a width of ¼ the web depth and a length of 50 mm (1.97 in). The results compared to FSM are listed in Table 3, where the average ratio was slightly more conservative and the standard deviation was similar to that for the sections without the holes. The analytical approach provides similar results to FSM using the same web thickness approximation.

A separate set of verifications were performed with the sections in Table 2 for bending about the major axis. The objective was to identify the equation set best suited for this prediction. Table 4 summarizes the results of these analyses.

Table 4: Prediction equation comparison for major axis bending

Equation Set:	1	2	3	4	5	6
$k_{\phi fe}$	2.3.1.3-3[a]	2.3.1.3-3[a]	2.3.1.3-3[a]	2.3.1.3-3[a]	2.3.1.3-3[a]	2.3.1.3-3[a]
$\tilde{k}_{\phi fg}$	2.3.1.3-5[a]	Eq. 15	Eq. 15	Eq. 15	Eq. 15	Eq. 16
$k_{\phi we}$	2.3.3.3-5[a]	2.3.3.3-5[a]	Eq. 46	Eq. 46	Eq. 46	Eq. 46
$\tilde{k}_{\phi wg}$	2.3.3.3-6[a]	2.3.3.3-6[a]	2.3.3.3-6[a]	Eq. 49	Eq. 48	Eq. 49
F_{pred}/F_{FSM}	0.925	0.948	0.967	0.966	0.982	0.987
Std Dev	0.096	0.086	0.097	0.096	0.106	0.087

[a] AISI (2016) Equation

Equation set 1 represents the current AISI provisions. Equation set 2 implements Eq. 15 for $\tilde{k}_{\phi fg}$, which improves the average prediction and reduces the standard deviation. Equation set 3 incorporates Eq. 46 for $k_{\phi we}$, which also improves the prediction but with a slightly higher standard deviation. Equation set 4 utilizes Eq. 49 for $\tilde{k}_{\phi wg}$ which is a minor simplification to the AISI equation without loss of accuracy.

Equation set 5 uses Eq. 48 in place of Eq. 49, which improves the average prediction but with a slightly higher standard deviation. Finally, equation set 6 is the same as equation set 4, but uses Eq. 16 to adjust $\tilde{k}_{\phi fg}$ for the stress at the centroid of the flange. This provides the greatest accuracy but adds complexity.

Impact on Design

The lack of specific distortional buckling provisions for minor axis bending makes it unlikely this failure mode is considered in common design practice. A study was performed to determine the impact of distortional buckling on the design strength, which is summarized in Table 5.

The Steel Stud Manufacturers Association (SSMA) publishes a technical guide (2015) containing standardized stud shapes with web holes. These shapes were analyzed using equation set 3 as defined in Table 3 to determine the minor axis elastic distortional buckling bending stress. The AISI (2016) provisions were then used to calculate the nominal flexural strength M_{nd}. This was compared to the nominal minor axis flexural strength for yielding and local buckling M_{nlo}.

Table 5: Impact on SSMA structural studs

	Grade 33	Grade 50
Number of sections	241	189
Sections controlled by M_{nd}	169	161
Average M_{nd}/M_{nlo}	0.834	0.789
Minimum M_{nd}/M_{nlo}	0.701	0.617

About ¾ of the sections were controlled by distortional buckling, and of those the average strength reduction was nearly 20%. Several sections had a strength reduction of more than 25%. The Grade 50 sections were impacted more than the Grade 33 sections. These results demonstrate the need to explicitly address this failure mode in design specifications.

Conclusions

Distortional buckling can be a controlling failure mode for minor axis bending of channel sections, hat sections, and many other shapes, where a stress gradient exists in the flanges. Current design specifications do not explicitly address this buckling mode, which could result in unsafe designs.

An analytical method was developed to predict the elastic distortional buckling stress. The method was verified for simple lip stiffeners, intermediates stiffeners, complex stiffeners, and perforated webs. Comparisons were made to finite strip solutions with reliable results.

This analytical approach is consistent with other AISI distortional buckling provisions, permitting a clean implementation for bending about the axis perpendicular to the flange. The flange/web rotational stiffness components defined as equation set 3 in Table 3 are recommended for inclusion in the AISI Specification.

In addition, the current AISI equations for distortional buckling of flexural members bending about the axis perpendicular to the web were reviewed. Some opportunities for simplification and improvement in accuracy were identified. The flange/web rotational stiffness components defined as equation set 4 in Table 4 are recommended as modifications to the current AISI provisions.

Notation

A_f	Cross-sectional area of flange
C_{wf}	Torsional warping constant of flange
E	Modulus of elasticity
e_x, e_y	Eccentricity of axial force in the *x* and *y* directions
f_1	Bending stress at extreme compression fiber of flange
f_2	Bending stress at flange/web juncture
f_3	Bending web stress opposite the flange/web juncture
f_{cg}	Bending stress at centroid of flange
f_{crd}	Critical distortional buckling stress
G	Shear modulus of elasticity
h	Web depth
I_{of}	Polar moment of inertia of flange about x and y axes
I_{xf}, I_{yf}	Moment of inertia of flange about x and y axes
I_{xyf}	Product of inertia of flange about x and y axes
J_f	Saint-Venant torsion constant for flange
$k_{\phi f}$	Rotational stiffness demanded by the flange
$k_{\phi fe}$, $\tilde{k}_{\phi fg}$	Elastic and geometric components of flange rotational stiffness
$k_{\phi w}$	Rotational stiffness provided by the web
$k_{\phi we}$, $\tilde{k}_{\phi wg}$	Elastic and geometric components of web rotational stiffness
k_{ije}, k_{ijg}	Finite strip coefficients for elastic and geometric stiffness
L	Distortional buckling half-wavelength
M_1, M_2	Nodal moments at edges of web finite strip
P	Axial force on flange producing stress gradient
R_y	Reaction force on flange provided by web at flange/web juncture
u, v	Flange buckling displacement in x and y directions
ϕ	Flange buckling angle of twist
x_c	x coordinate of extreme compression fiber of flange relative to flange centroid
x_h	x coordinate of flange/web juncture relative to flange centroid
x_{of}, y_{of}	Coordinates of shear center of flange relative to centroid of flange
β_{xf}, β_{yf}	Geometric properties of flange cross-section used for beam-column flexural-torsional buckling determination
μ	Poisson's ratio
θ_1, θ_2	Node rotations at edges of web finite strip
ξ_f	Flange stress gradient
ξ_w	Web stress gradient
ψ_f	Flange stress ratio

References

American Iron and Steel Institute (2016), *North American Specification for the Design of Cold-Formed Steel Structural Members*, 2016 Edition, Washington, DC, 2016.

Cheung, Y.K. (1976), *Finite Strip Method in Structural Analysis*, Pergamon Press, New York, 1976.

Glauz, R.S. (2017a), "Elastic lateral-torsional buckling of general cold-formed steel beams under uniform moment," *Thin-Walled Structures*, Vol. 119, October 2017.

Glauz, R.S. (2017b), "Flexural-torsional buckling of general cold-formed steel columns with unequal unbraced lengths," *Thin-Walled Structures*, Vol. 119, October 2017.

Lau, S.C.W. and Hancock, G.J. (1987), "Distortional Buckling Formulas for Channel Columns," *Journal of Structural Engineering*, Vol. 113, May 1987.

Hancock, G.J. (1995), "Design for Distortional Buckling of Flexural Members," *Proceedings of the Third International Conference on Steel and Aluminum Structures*, Istanbul Turkey, May 1995.

Hancock, G.J. (1997), "Design for Distortional Buckling of Flexural Members," *Thin-Walled Structures*, Vol. 27, 1997.

Peköz, T.B. and Winter, G. (1969), "Torsional Flexural Buckling of Thin-Walled Sections under Eccentric Load," *Journal of the Structural Division*, ASCE, Vol. 95, May 1969.

Schafer, B.W. and Peköz, T. (1999), "Laterally Braced Cold-Formed Steel Flexural Members with Edge Stiffened Flanges," *Journal of Structural Engineering*, Vol. 125, February 1999.

Schafer, B.W. (2002), "Local, Distortional, and Euler Buckling of Thin-Walled Columns," *Journal of Structural Engineering*, Vol. 128, March 2002.

Schafer, B.W., Sarawit, A. and Peköz, T. (2006), "Complex Edge Stiffeners for Thin-Walled Members," *Journal of Structural Engineering*, Vol. 132, February 2006.

Steel Stud Manufacturers Association (2015), *Product Technical Guide*, SSMA, Chicago, IL, 2015.

Teng, J.G., Yao, J., and Zhao, Y. (2003), "Distortional buckling of channel beam-columns," *Thin-Walled Structures*, Vol. 41, 2003.

Timoshenko, S. and Woinowsky-Krieger, S. (1959), *Theory of Plates and Shells*, 2nd Edition, McGraw-Hill, New York, NY, 1959.